





Original Article

Praja1 RING-finger E3 ubiquitin ligase is a common suppressor of neurodegenerative disease-associated protein aggregation

Kazuhiko Watabe,^{1,2}  Motoko Niida-Kawaguchi,^{2,3} Mari Tada,⁴ Yoichiro Kato,²  Makiko Murata,¹ Kunikazu Tanji,⁵ Koichi Wakabayashi,⁵  Mitsunori Yamada,⁶ Akiyoshi Kakita⁴ and Noriyuki Shibata² 

Departments of ¹Medical Technology (Neuropathology), Faculty of Health Sciences, ²Clinical Psychology, Faculty of Health Sciences, Kyorin University, ³Division of Pathological Neuroscience, Department of Pathology, Tokyo Women's Medical University, Tokyo, ⁴Department of Pathology, Brain Research Institute, Niigata University, Niigata, ⁵Department of Neuropathology, Institute of Brain Science, Hirosaki University Graduate School of Medicine, Hirosaki and ⁶Division of Neuropathology, Department of Brain Disease Research, Shinshu University School of Medicine, Matsumoto, Japan

The formation of misfolded protein aggregates is one of the pathological hallmarks of neurodegenerative diseases. We have previously demonstrated the cytoplasmic aggregate formation of adenovirally expressed transactivation response DNA-binding protein of 43 kDa (TDP-43), the main constituent of neuronal cytoplasmic aggregates in cases of amyotrophic lateral sclerosis (ALS) and frontotemporal lobar degeneration (FTLD), in cultured neuronal cells under the condition of proteasome inhibition. The TDP-43 aggregate formation was markedly suppressed by co-infection of adenoviruses expressing heat shock transcription factor 1 (HSF1), a master regulator of heat shock response, and Praja1 RING-finger E3 ubiquitin ligase (PJA1) located downstream of the HSF1 pathway. In the present study, we examined other reportedly known E3 ubiquitin ligases for TDP-43, i.e. Parkin, RNF112 and RNF220, but failed to find their suppressive effects on neuronal cytoplasmic TDP-43 aggregate formation, although they all bind to TDP-43 as verified by co-immunoprecipitation. In contrast, PJA1 also binds to adenovirally expressed wild-type and mutated fused in sarcoma, superoxide dismutase 1, α -synuclein and ataxin-3,

and huntingtin polyglutamine proteins in neuronal cultures and suppressed the aggregate formation of these proteins. These results suggest that PJA1 is a common sensing factor for aggregate-prone proteins to counteract their aggregation propensity, and could be a potential therapeutic target for neurodegenerative diseases that include ALS, FTLD, Parkinson's disease and polyglutamine diseases.

Key words: fused in sarcoma, Praja1, superoxide dismutase 1, transactivation response DNA-binding protein of 43 kDa, α -synuclein.

INTRODUCTION

Protein aggregation and spreading are prominent features of neurodegenerative diseases such as prion disease, Alzheimer's disease, frontotemporal lobar degeneration (FTLD), Huntington's disease (HD), Parkinson's disease (PD), spinocerebellar degeneration (SCD) and amyotrophic lateral sclerosis (ALS).^{1–7} Among these, transactivation response DNA-binding protein of 43 kDa (TDP-43) is the main component of cytoplasmic aggregates demonstrated in neurons and glial cells in patients with ALS and FTLD.^{8–13} In ALS and FTLD, wild-type (WT) TDP-43 is cleaved, and a resultant 25-kDa C-terminal fragment (CTF) that lacks nuclear localization signal is localized to the cytoplasm. Cytoplasmic TDP-43 aggregates are composed of WT and CTF TDP-43, and are phosphorylated and ubiquitinated.^{8–11} We have previously shown that adenoviruses expressing human WT and CTF TDP-43 induce the cytoplasmic TDP-43 aggregate formation in cultured

Correspondence: Kazuhiko Watabe, MD, PhD, Department of Medical Technology (Neuropathology), Kyorin University Faculty of Health Sciences, 5-4-1 Shimorenjaku, Mitaka, Tokyo 181-8612, Japan. Email: watabe@ks.kyorin-u.ac.jp

Received 15 March 2022; revised 16 May 2022; accepted 17 May 2022; published online 14 June 2022.

© 2022 The Authors. *Neuropathology* published by John Wiley & Sons Australia, Ltd on behalf of Japanese Society of Neuropathology.

This is an open access article under the terms of the [Creative Commons Attribution-NonCommercial-NoDerivs](https://creativecommons.org/licenses/by-nc-nd/4.0/) License, which permits use and distribution in any medium, provided the original work is properly cited, the use is non-commercial and no modifications or adaptations are made.

neuronal cells under proteasome inhibition.^{14,15} We have also demonstrated that co-infection of an adenovirus expressing heat shock transcription factor 1 (HSF1), a master regulator of heat shock response, markedly suppressed the formation of adenoviral TDP-43 aggregates.¹⁶ To identify candidate molecules located downstream of HSF1, we performed DNA microarray analysis and revealed that Praja 1 RING-finger E3 ubiquitin ligase (PJA1) inhibits TDP-43 phosphorylation and aggregate formation.¹⁶

Ubiquitin ligase activities for TDP-43 have been previously identified that include Parkin/PARK2,¹⁷ the von Hippel-Lindau (VHL)/cullin-2 (CUL2) E3 complex,¹⁸ RNF112/ZNF179¹⁹ and RNF220.²⁰ Accordingly, in the present study, we compared suppressive effects of PJA1, Parkin, RNF112 and RNF220 on adenoviral TDP-43 aggregate formation in our cultured neuronal cell models. On the other hand, Ghosh *et al.*²¹ recently demonstrated that PJA1 also facilitates the degradation of polyglutamine proteins, i.e. ataxin-3 and huntingtin, and suppresses polyglutamine-mediated toxicity, which suggests a possibility of common suppressive activity of PJA1 on the formation of protein aggregates in neurodegenerative diseases. In the present study, we examined whether PJA1 suppresses the adenovirus-induced aggregate formation of representative proteins in ALS, FTL, PD, SCD and HD that include TDP-43, fused in sarcoma (FUS), superoxide dismutase 1 (SOD1), α -synuclein, and ataxin-3 and huntingtin polyglutamine proteins in our cultured neuronal cell models.

MATERIALS AND METHODS

Cell culture

All experiments were performed following Japanese National Guidelines and Regulations, and were approved by the Biosafety Committee (#164-6) and the Animal Care and Use Committee (#117-01-04) of Kyorin University Faculty of Health Sciences. The adult rat neural stem cell line 1464R that we have established (Cat. No. #T0746; Applied Biological Materials, Canada, Cat. No. #RNSCL-C; Cosmo Bio, Tokyo, Japan) was cultured as previously described.^{14-16,22} To differentiate 1464R cells into neuronal and glial cells, dissociated 1464R cells were seeded on poly-L-lysine (PLL; #P1524; Sigma-Aldrich, St Louis, MO, USA)-coated 12-well plates or 9-mm ACLAR round coverslips (Allied Fibers & Plastics, Pottsville, PA, USA) at a density of $4-6 \times 10^5$ cells per well and $1-2 \times 10^4$ cells per coverslip, respectively, and maintained in differentiation medium composed of F12 medium (Cat. No. #11765-054; Thermo Fisher Scientific, Waltham, CA, USA) containing 5% fetal bovine serum (Moregate, Bulimba, Australia), 0.5% N2 supplement (Cat. No. #17502-048; Thermo Fisher), 1% B27 supplement (Cat. No. #17504-044; Thermo Fisher), $1 \mu\text{M}$ all-trans retinoic acid (ATRA; Cat.

No. # R2625; Sigma-Aldrich), 50 units/mL penicillin and 50 $\mu\text{g}/\text{mL}$ streptomycin in 5% CO_2 at 37°C.

Adenovirus infection

Preparation of adenovirus vectors expressing 5'-DsRed-tagged full-length human WT (1-414 aa) and CTF (208-414 aa) TDP-43 fused with FLAG tag at the 3'-ends (AxDsRhTDP43WTFL, AxDsRhTDP43CTFFL), 3'-EGFP-tagged human WT HSF1 (AxBHSF1EGFP) and human WT (variant V1; 1-643 aa) and RING finger domain-lacking (Δ R) PJA1 (AxBPJA1EGFP, AxBPJA1 Δ REGFP) have been previously described¹⁶ (Fig. 1). For the construction of adenovirus vectors expressing 3'-EGFP tagged WT Parkin (AxBPRKNEGFP), RNF112/ZNF179 (AxBRNF112EGFP) and RNF220 (AxBRNF220EGFP), and 5'-DsRed- and 3'-FLAG-tagged WT and P525L FUS (AxDsRhFUSWTFL, AxDsRhFUSP525LFL), WT and G93A SOD1 (AxDsRhSOD1WTFL, AxDsRhSOD1G93AFL), WT and A53T α -synuclein (AxDsRhSNCAWTFL, AxDsRhSNCAA53TFL), ataxin-3 Q28 and Q84 (AxDsRhATXN3-Q28FL, AxDsRhATXN3Q84FL), and Htt exon 1 Q23 and Q74 (AxDsRhHttEx1Q23FL, AxDsRhHttEx1Q74FL), cDNAs obtained from HEK 293 cells by reverse transcription polymerase chain reaction (RT-PCR) or from Addgene plasmids pEGFP-C1-Ataxin3 Q28 (Cat. No. #22122; Addgene, Watertown, MA, USA), pEGFP-C1-Ataxin3 Q84 (Cat. No. #22123; Addgene), pEGFP-Q23 (Cat. No. #40261; Addgene) and pEGFP-Q74 (Cat. No. #40262; Addgene) by PCR using primers as listed in Table 1 were cloned into pEGFPN1-3 and DsRed-Monomer-C1 (Clontech, Palo Alto, CA, USA), respectively, and *Swa*I cloning site of adenovirus cassette cosmid pAxCawtit2 (Cat. No. #6170; TaKaRa, Osaka, Japan) as described^{14-16,22} (Fig. 1A, B). Point mutations of SOD1 (G93A:g281c) and α -synuclein (A53T:g157a) were created by QuikChange II Site-Directed Mutagenesis Kit (Agilent Technologies, Santa Clara, CA, USA). C-terminal point mutation of FUS (P525L:c1574t) was introduced by conventional PCR (Table 1) using WT FUS as a template. For the construction of adenoviruses encoding shRNAs and EGFP, shRNA sequences for rat negative control¹⁴ and rat PJA1 (XM_006257105; GCTGGACGGA-AACAACAAT) were cloned into pGeneClip hMGFP (Promega, Madison, WI, USA) in which hMGFP fragment was replaced by EGFP fragment, and the resulting U1-shRNA/CMV-EGFP fragment was subcloned into *Swa*I site of a cassette cosmid pAxcwit2 (Cat. No. #6170; TaKaRa) as described¹⁴ (Fig. 1C). The cosmids were then transfected to 293 cells, and recombinant adenoviruses were amplified and harvested in the form of culture media. Differentiated 1464R cells on PLL-coated 12-well plates or 9-mm coverslips were infected with the adenoviruses at a multiplicity of infection (MOI) of 50. Twenty-four hours later, the cells were

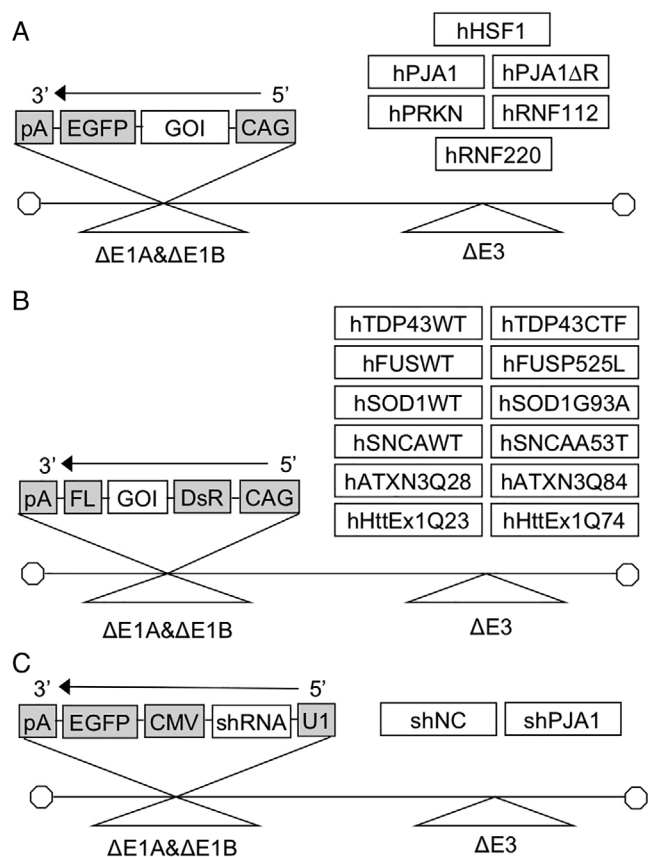


Fig. 1 Schematic diagram of recombinant adenovirus vectors encoding 3'-EGFP-tagged gene of interest (GOI), i.e. human wild-type (WT) HSF1 (AxsHSF1EGFP), WT and RING finger domain-lacking (Δ R) PJA1 (AxsPJA1EGFP, AxsPJA1 Δ REGFP), WT Parkin (AxsPRKNEGFP), WT RNF112 (AxsRNF112EGFP) and WT RNF220 (AxsRNF220EGFP) (A), and 5'-DsRed (DsR)- and 3'-FLAG (FL)-tagged GOI, i.e. human WT and C-terminal fragment (CTF) TDP-43 (AxDsRhTDP43WTFL, AxDsRhTDP43CTFFL), WT and P525L FUS (AxDsRhFUSWTFL, AxDsRhFUSP525LFL), WT and G93A SOD1 (AxDsRhSOD1WTFL, AxDsRhSOD1G93AFL), WT and A53T α -synuclein (AxDsRhSNCAWTFL, AxDsRhSNCAA53TFL), ataxin-3 Q28 and Q84 (AxDsRhATXN3Q28FL, AxDsRATXN3Q84FL), and huntingtin exon 1 Q23 and Q74 (AxDsRhHttEx1Q23FL, AxDsRhHttEx1Q74FL) (B), and shRNAs for rat negative control (NC) and rat PJA1 coupled with EGFP (AxsNC/EGFP, AxsPJA1/EGFP) (C). These vectors contain the adenovirus type-5 genome lacking the E1A, E1B (Δ E1A& Δ E1B) and E3 (Δ E3) regions to prevent the virus replication, the cytomegalovirus early enhancer/chicken β -actin (CAG), U1 or cytomegalovirus (CMV) promoter on the 5' end, and the rabbit β -globin polyA sequence (pA) on the 3' end.

exposed to 0.5 μ M MG-132 (Cat. No. #474790; Merck Millipore, Burlington, MA, USA) and further incubated for 24 h. In some experiments, proteasome inhibitors lactacystin (Cat. No. #426100; Merck Millipore) and bortezomib (Cat. No. #021-18 901; FUJI FILM Wako, Osaka, Japan) were used in place of MG-132.

Cell fractionation, co-immunoprecipitation (Co-IP) and Western blotting

For cell fractionation, cultured cells in 12-well plates ($4-5 \times 10^5$ cells/well) were lysed, sonicated and centrifuged at 20 000 g for 90 min at 4°C as described.¹⁶ The supernatants and pellets were collected as RIPA-soluble and -insoluble fractions, respectively, lysed in 1 \times SDS-sample buffer containing 2-mercaptoethanol (2-ME) and treated for 5 min at 95°C. Other conventional cell lysates for shRNA experiments were prepared by centrifugation at 12 000 g for 20 min at 4°C. The protein concentration of each supernatant fraction was determined with Qubit Protein Assay kit (Thermo Fisher).

For Co-IP, 1464R cells in 12-well plates (6×10^5 cells/well) were lysed, sonicated and centrifuged at 12 000 g for 30 min at 4°C as described.¹⁶ Ten percent of the resulting supernatants were analyzed as the input cell lysate, and the remaining 90% of supernatants were immunoprecipitated with anti-FLAG M2 affinity gel (Cat. No. #A2220; Sigma-Aldrich). The inputs and immunoprecipitates were lysed in 1 \times SDS-sample buffer containing 2-ME and treated for 5 min at 95°C.

Fractionated cell lysates (10–20 μ g) or immunoprecipitates were electrophoresed on 4–20% SDS/polyacrylamide gels under reduced conditions and transferred to polyvinylidene difluoride (PVDF) membrane (Atto, Tokyo, Japan). The blotted membrane was pretreated with 3% skim milk and incubated overnight at 4°C with rabbit polyclonal anti-phosphorylated TDP-43 (pSer409/S410; Cat. No. #TIP-PTD-P02; Cosmo Bio), rabbit polyclonal anti-TDP-43 C-terminus (405–414; Cat. No. #TIP-TD-P09; Cosmo Bio), rabbit polyclonal anti-FLAG (Cat. No. #F7425; Sigma-Aldrich, St Louis, MO, USA), rabbit polyclonal anti-green fluorescent protein (GFP; Cat. No. #ab6446; Abcam, Cambridge, UK), rabbit polyclonal anti-PJA1 (Cat. No. #17687-1-AP; ProteinTech Japan, Japan), rabbit monoclonal anti-ubiquitin K48 (Apu2; Cat. No. #05-1307; Sigma-Aldrich), rabbit polyclonal anti-PRKN/PARK2 (Cat. No. #14060-1-AP; ProteinTech), rabbit polyclonal anti-ZNF179 (Cat. No. #ab246912; Abcam), rabbit polyclonal anti-RNF220 (Cat. No. #HPA027578; Sigma-Aldrich), rabbit polyclonal anti-FUS (Cat. No. #11570-1-AP; ProteinTech), rabbit polyclonal anti-SOD1 (Cat. No. #10269-1-AP; ProteinTech), rabbit polyclonal anti- α -synuclein (Cat. No. #10842-1-AP; ProteinTech), mouse monoclonal anti-phosphorylated α -synuclein (pSyn#64; Cat. No. #015-25 191; FUJIFILM Wako Pure Chemicals, Osaka, Japan), mouse monoclonal anti-ataxin 3 (1H9; Cat. No. #MAB5376; Merck Millipore), mouse monoclonal anti-polyglutamine (5TF-1C2; Cat. No. #MAB1574; Merck Millipore) and mouse monoclonal anti-GAPDH (Cat. No. #ab8245; Abcam) antibodies at dilutions of 1:1000, followed by incubation with biotinylated anti-

Table 1 PCR primers used in this study (F: forward, R: reverse)

Gene (h:human)	Primer
hPRKN (NM_004562)	F: CGAAGCTTGCCACCATGATAGTGTGGTTCAGGTTCC R: TGAATTCCACGTCGAACCAGTGGTCCCCCA
hRNF112 (NM_007148)	F: ATAAGCTTGCCACCATGCCAAGGCCCGCCTTGTCA R: TGAATTCCTCTTCCTGGAGAAGGGGCTCTCGGTCC
hRNF220 (NM_018150)	F: ATAAGCTTGCCACCATGGACTTACACCGGGCAGCC R: ATGGATCCACAAGTAGATCCTCCGCAGGTCTCCGG
hFUS/FLAG (NM_018150)	F: CGGTACCATGGCCTCAAACGATTATACCCAACAAGCAACC R: TAGGATCCTACTTGTTCATCGTCGTCCTTGTAGTCATACGGCCTCTCCCT
hFUSP525L/FLAG (NM_004960)	F: CGGTACCATGGCCTCAAACGATTATACCCAACAAGCAACC R: TAGGATCCTACTTGTTCATCGTCGTCCTTGTAGTCATACAGCCTCTCCCT
hSOD1/FLAG (NM_000454)	F: ATAAGCTTATATGGCGACGAAGGCCGTGTGCGTGTGAAG R: TGGTACCTTACTTGTTCATCGTCGTCCTTGTAGTCTTGGGCGATCCCAAT
hSNCA/FLAG (NM_000345)	F: GCAAGCTTCGATGGATGTATTCATGAAAGGACTTTCAAAGGCCAAGGAG R: TGGTACCTTACTTGTTCATCGTCGTCCTTGTAGTCGGCTTCAGGTTTCGTA
hATXN3/FLAG (NM_001024631)	F: GCAAGCTTCGATGGAGTCCATCTTCCACGAGAAAC R: TGGTACCTTACTTGTTCATCGTCGTCCTTGTAGTCTGTGAAGGTAGCGAA
hHitEx1/FLAG (NM_001388492)	F: ATAAGCTTCGATGAAGGCCTTCGAGTCCCTCAAGT R: TGGTACCTTACTTGTTCATCGTCGTCCTTGTAGTCGACTGCAGAATTCGG

rabbit or anti-mouse IgG (Vector Laboratories, Burlingame, CA, USA; 1:1000) for 1 h and streptavidin-alkaline phosphatase (Cat. No. #11089161001; Sigma-Aldrich; 1:1000) for 1 h. Reactions were visualized by color development using nitroblue tetrazolium chloride (NBT) and 5-bromo-4-chloro-3-indolylphosphate p-toluidine salt (BCIP; Cat. No. #11681451001; Sigma-Aldrich). In some experiments, immunoblotted bands were quantified by ImageJ software (NIH, USA).

Immunocytochemistry

Cells were fixed with 4% paraformaldehyde (PFA) in phosphate-buffered saline (PBS), postfixed with 100% methanol, and immunostained with mouse monoclonal TuJ1 (Cat. No. #MAB1195; R&D systems, Minneapolis, MN, USA; 1:200), followed by incubations with Alexa Fluor 350-conjugated goat anti-mouse antibody (Thermo Fisher; 1:400) and Hoechst 33342 (Thermo Fisher; 2 µg/mL) as described previously.¹⁶ The cells were examined under an Olympus BX53 microscope equipped with a DP70 CCD camera.

Immunohistochemistry on human tissue sections

All experiments were approved by and performed under the guidelines of the Kyorin University Ethics Committee and Niigata University Ethics Committee. Informed consent was obtained from all individuals or their guardians before the autopsy analysis. Postmortem brain and spinal cord specimens from patients with a definite diagnosis of SOD1-ALS, PD, HD and Machado–Joseph disease (MJD; spinocerebellar ataxia type 3) and non-diseased control cases were fixed with

10% buffered formalin and embedded in paraffin. Deparaffinized and rehydrated sections were microwaved in citrate buffer, pH 6.0 for PJA1 immunostaining, or treated with formic acid for polyglutamine immunostaining as described below.

For light microscopic immunohistochemistry, serial 4-µm-thick deparaffinized sections were treated in 3% hydrogen peroxide, blocked with 5% skim milk/PBS, and incubated overnight with rabbit anti-PJA1 (Cat. No. #HPA000595; Atlas Antibodies, Bromma, Sweden; 1:100) or mouse monoclonal anti-polyglutamine (5TF-1C2; Cat. No. #MAB1574; Merck Millipore; 1:16 000) antibody, followed by incubation with Histofine polymer-immunocomplex for 1 h (Nichirei, Tokyo, Japan). The sections were incubated with 3,3'-diaminobenzidine tetrahydrochloride, counterstained with hematoxylin, and examined under the Olympus BX53 microscope equipped with a DP71 CCD camera.

For double immunofluorescence, deparaffinized sections were blocked with 10% normal goat serum and incubated overnight with a mixture of rabbit anti-PJA1 (Cat. No. #HPA000595; Atlas Antibodies; 1:100) and mouse monoclonal anti-polyglutamine (5TF-1C2; Cat. No. #MAB1574; Merck Millipore; 1:8000), followed by incubation with a mixture of Alexa 488-conjugated goat anti-rabbit and Alexa 568-conjugated goat anti-mouse antibodies (Molecular Probes, Eugene, OR, USA) at dilutions of 1:400 for 1 h. The sections were treated with Autofluorescence Eliminator Reagent (Cat. No. #2160; Merck Millipore) as described,¹⁶ mounted with VECTASHIELD® mounting medium with 4',6-diamidino-2-phenylindole (DAPI) nuclear stain (Vector), and examined under a Carl Zeiss LSM700 confocal laser-scanning microscope.

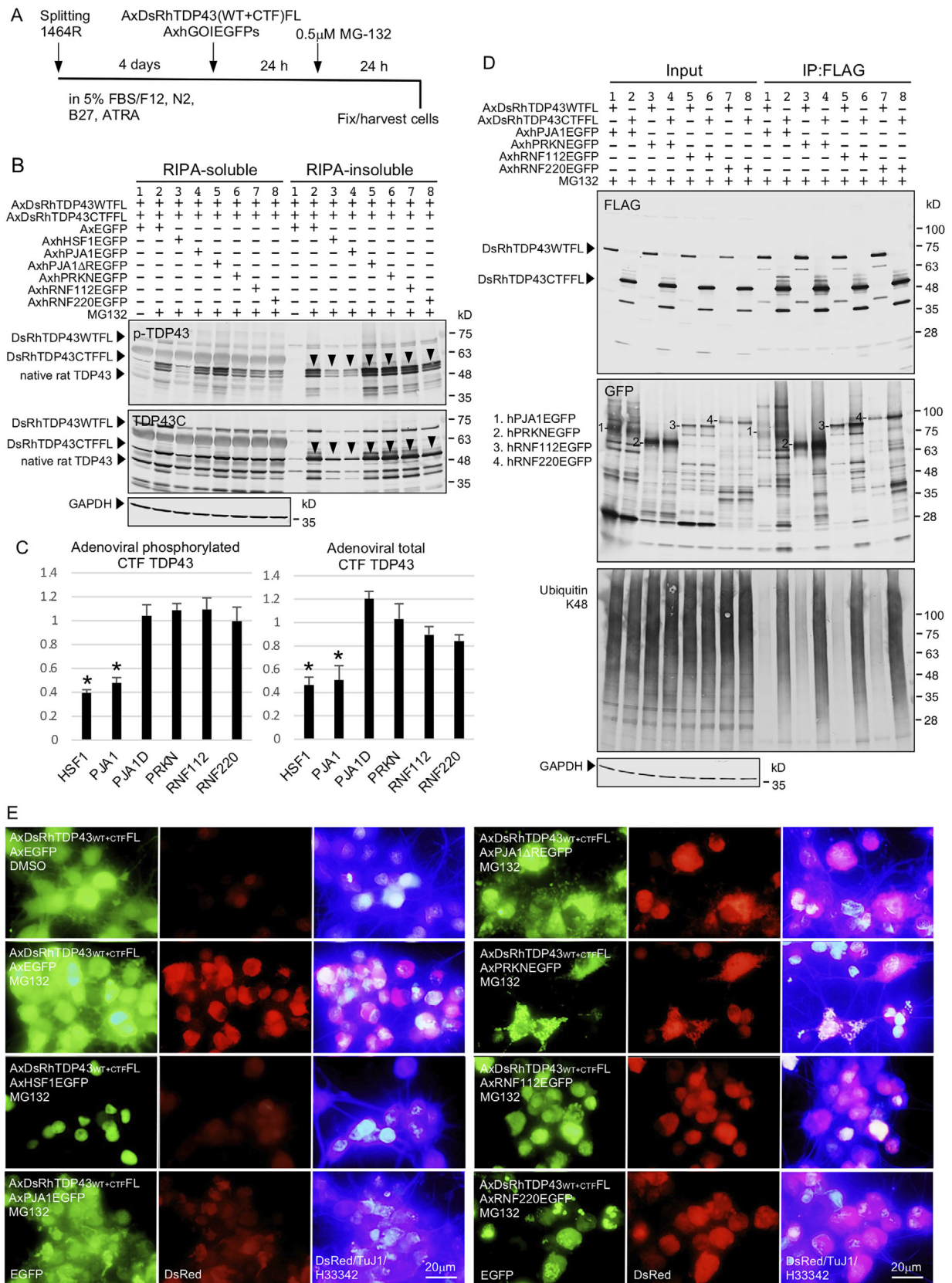


Fig. 2 Suppressive effects of E3 ubiquitin ligases on neuronal TDP-43 aggregate formation. (A) Schematic presentation of the experiments for adenoviral TDP-43 aggregate formation. The differentiated 1464R cells were infected with adenoviruses expressing DsRed- (Figure legend continues on next page.)

Statistics

The data in each group were expressed as the mean \pm SD. An unpaired Student's *t*-test was used for comparisons between two groups. Data in three–eight groups were compared by one-way analysis of variance and post hoc Bonferroni correction. A *P*-value less than 0.05 was considered statistically significant.

RESULTS

Suppressive effects of E3 ubiquitin ligases on neuronal TDP-43 aggregate formation

We have previously demonstrated the formation of cytoplasmic TDP-43 aggregates in rat 1464R neural stem cell-derived neurons induced by recombinant adenoviruses expressing human WT and CTF TDP-43 under proteasomal inhibition.^{14,15} These TDP-43 aggregates showed strong immunoreactivity for phosphorylated TDP-43, p62 and ubiquitin, and were detected in RIPA-insoluble fractions by Western blot analysis, recapitulating key biochemical features of pathological TDP-43 aggregates found in human ALS and FTL.^{14,15} The TDP-43 aggregate formation was significantly suppressed by infection of adenoviruses expressing HSF1 and PJA1 located downstream of the HSF1 pathway.¹⁶ In the present study, we then investigated suppressive effects of other reportedly known E3 ubiquitin ligases for TDP-43, i.e. Parkin/PARK2,¹⁷ RNF112/ZNF179¹⁹ and RNF220,²⁰ on TDP-43 aggregate formation. The differentiated 1464R cells were infected with adenoviruses expressing DsRed- and FLAG-tagged human WT and CTF TDP-43 in the presence of a proteasome inhibitor MG-132 (Fig. 2A). Western blot analysis demonstrated that when the cells were co-infected with adenoviruses expressing PJA1, Parkin, RNF112 and RNF220 (Fig. 2A), only PJA1 adenovirus infection reduced the amount of RIPA-insoluble, phosphorylated TDP-43 fraction (Fig. 2B, C), although all these ubiquitin ligases were co-immunoprecipitated with adenoviral WT and CTF TDP-43 that were ubiquitinated (Fig. 2D). Fluorescence microscopy revealed DsRed-positive dense

cytoplasmic aggregates in TuJ1-immunoreactive neurons induced by WT and CTF TDP-43 adenoviruses in the presence of MG-132, which was markedly suppressed by co-infection of adenoviruses expressing HSF1 and PJA1, but not Parkin, RNF112 or RNF220 (Fig. 2E). These results indicate that PJA1, but not Parkin, RNF112 or ZNF220, is one of the major E3 ubiquitin ligases for TDP-43 to reduce its aggregation propensity in the present neuronal cell experiments.

PJA1 suppresses the aggregate formation of neurodegenerative disease-associated proteins

Our previous report¹⁶ describing suppressive effects of PJA1 on TDP-43 aggregate formation was followed by the recent report of Ghosh *et al.*²¹ demonstrating that PJA1 also facilitates degradation of ataxin-3 and huntingtin polyglutamine proteins and reduces polyglutamine-mediated toxicity, which suggests a possibility of common suppressive activity of PJA1 on the formation of protein aggregates in neurodegenerative diseases. We, therefore, examined the suppressive effects of the PJA1 adenovirus on the insoluble aggregate formation of adenovirus-induced FUS, SOD1, α -synuclein, ataxin-3 and huntingtin in the differentiated 1464R neurons. The 1464R cells were differentiated as above, and co-infected with adenoviruses expressing DsRed- and FLAG-tagged human WT or P525L FUS, WT or G93A SOD1, WT or A53T α -synuclein, ataxin-3 Q28 or Q84, or huntingtin exon 1 Q23 or Q74, and EGFP-tagged WT PJA1 or PJA1 Δ R in the presence of MG-132 (Fig. 3A). Western blot analysis of RIPA-soluble and -insoluble fractions demonstrated that, as a whole, RIPA-insoluble fractions of both of these WT and mutated proteins are significantly decreased by co-infection of PJA1, but not PJA1 Δ R, adenovirus (Fig. 3B–E1,2). Despite lacking the RING-finger domain, PJA1 Δ R adenovirus also suppressed the aggregate formation of G93A SOD1 (Fig. 3C1,2) and the phosphorylation of WT and A53T α -synuclein (Fig. 3D1,2). Co-IP revealed that both PJA1 and PJA1 Δ R bind to all these WT and mutated proteins that were ubiquitinated regardless of

(Figure legend continued from previous page.)

and FLAG-tagged human wild-type (WT; AxDsRhTDP43WTFLL) and C-terminal fragment (CTF; AxDsRhTDP43CTFFL) TDP-43 and EGFP-tagged human genes of interest (GOIs; AxhGOIEGFPs, i.e. AxhHSF1EGFP, AxhPJA1EGFP, AxhPJA1 Δ REGFP, AxhPRKNEGFP, AxhRNF112EGFP or AxhRNF220EGFP), followed by incubation with 0.5 μ M MG-132. (B) Western blot analysis of suppressive effects of adenoviral HSF1 and E3 ubiquitin ligases on phosphorylation and aggregate formation of adenoviral TDP-43. (C) Densitometric analysis of the Western blot data of RIPA-insoluble phosphorylated and total CTF TDP-43 (arrowheads in B; *n* = 3) calibrated by GAPDH signals. Data are expressed as relative density compared with AxEGFP-treated control samples in the presence of MG-132. Results are presented as mean \pm SD. Statistical comparison was performed by a two-tailed unpaired *t*-test (**P* < 0.05). (D) The co-immunoprecipitation (Co-IP) assay showing that PJA1 (1), Parkin (2), RNF112 (3) and RNF220 (4) all bind to WT and CTF TDP-43 that are ubiquitinated. (E) Fluorescence microscopy of TuJ1-immunoreactive neurons infected with adenoviruses expressing DsRed-tagged human WT and CTF TDP-43 (AxhDsRTDP43_{WT}+CTFFL) and EGFP-tagged human HSF1, PJA1, PJA1 Δ R, Parkin (PRKN), RNF112 and RNF220 in the presence of MG-132. The nucleus was counterstained with Hoechst 33342.

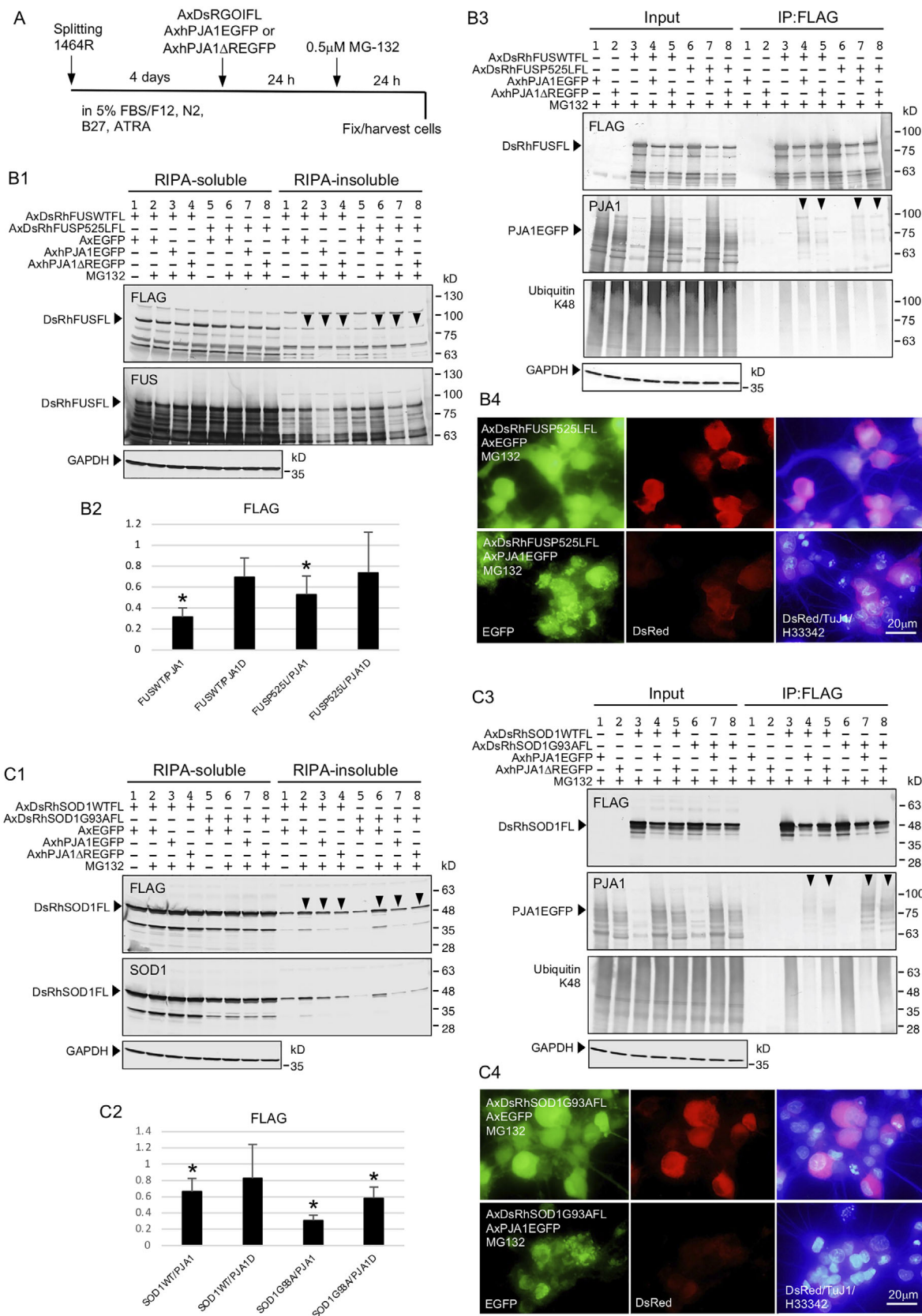


Fig. 3 Suppression of the aggregate formation of neurodegenerative disease-associated proteins by PJA1. (A) Schematic presentation of the experiments for adenovirus-transduced protein aggregate formation. The 1464R-derived neuronal cells were infected with (Figure legend continues on next page.)

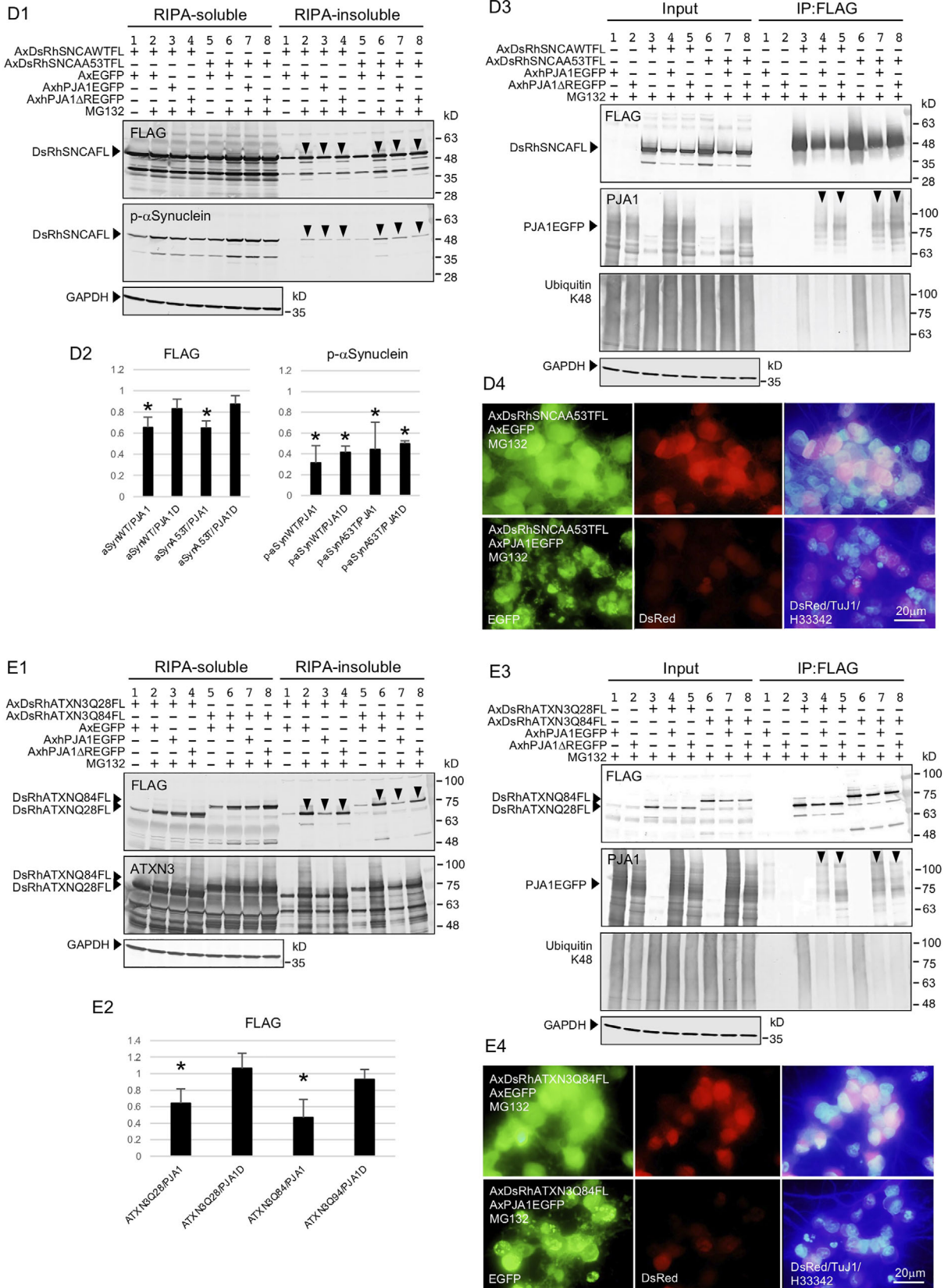


Fig. 3 (Figure legend continues on next page)

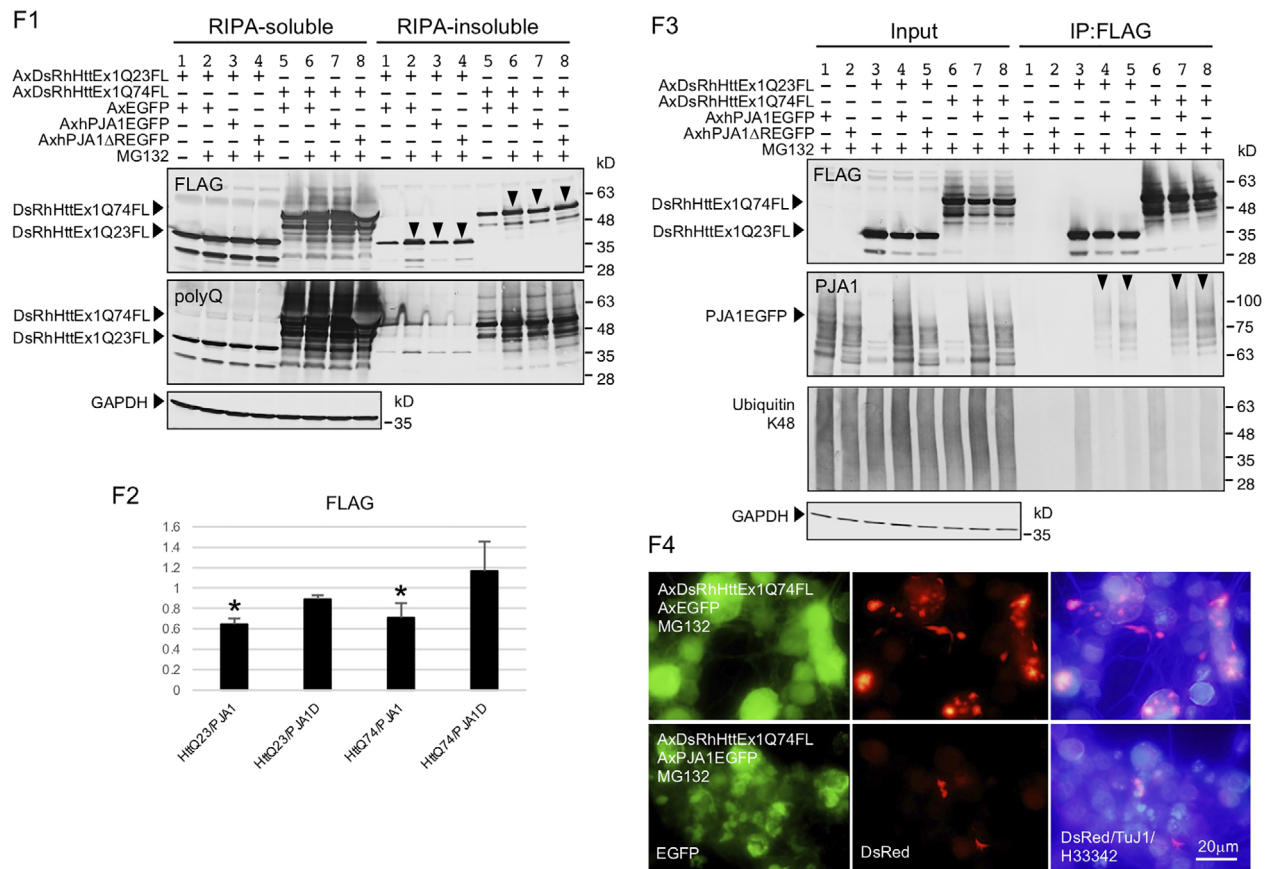


Fig. 3 (Figure legend continues on next page)

adenoviral PJA1 induction (Fig. 3B3–F3), probably because of the presence of endogenous PJA1 and/or other ubiquitin ligases that ubiquitinate these proteins in the Co-IP samples. Fluorescence microscopy showed decreased DsRed-positive cytoplasmic aggregates in TuJ1-immunoreactive neurons by co-infection of PJA1 adenovirus (Fig. 3B4–F4). Because there is a possibility that MG-132 has specific effects on protein aggregation that are not related to proteasome inhibition, we also investigated the effects of other proteasome inhibitors, i.e. lactacystin and bortezomib. They similarly induced the formation of RIPA-insoluble proteins, which was suppressed by adenoviral PJA1 transduction (Fig. 4), confirming the common suppressive effect of PJA1 on protein aggregate formation under the condition of proteasome inhibition as has been shown in the case of TDP-43 in our previous study.¹⁶

HSF1 suppresses the aggregate formation of neurodegenerative disease-associated proteins

It has been well established that HSF1 suppresses the aggregate formation of several neurodegenerative

disease-associated proteins^{23–25} that include TDP-43,^{16,26,27} SOD1,^{28–30} α -synuclein,^{31–33} ataxin-3^{34,35} and huntingtin.³⁶ Previously, we have demonstrated upregulation of endogenous PJA1 expression by adenoviral HSF1, and we identified PJA1 as a downstream effector molecule upregulated by HSF1 that counteracts TDP-43 aggregate formation.¹⁶ In the present study, we reconfirmed that adenovirally transduced HSF1 also suppresses the aggregate formation of WT and mutated TDP-43, FUS, SOD1, α -synuclein, ataxin-3 and huntingtin in our experimental protocols (Fig. 5A, B). We next examined whether PJA1 knock-down would counteract the suppressive effects of HSF1 on protein aggregate formation, provided that these effects are solely due to HSF1-induced PJA1. As shown in our previous study, PJA1 is known to be self-ubiquitinated and rapidly degraded by the proteasome, and the proteasome inhibitor MG-132 promoted the detection of endogenous PJA1, predominantly its shortest form (variant X4).¹⁶ The present study showed that rat PJA1 shRNA successfully downregulated endogenous PJA1 induced by HSF1 in the presence of MG-132 (Fig. 5C, D). However, PJA1 shRNA did not negate the suppressive effects of HSF1 (Fig. 5E, F),

suggesting that PJA1 does not act as a full substitute for HSF1.

Immunohistochemistry of PJA1 in human brains

We examined immunohistochemical expression of PJA1 in postmortem brain and spinal cord specimens from patients with SOD1-ALS, PD, HD and MJD, and non-diseased control cases. In non-diseased control cases, the majority of neuronal cells including cortical, nigral, hippocampal, cerebellar and spinal cord neurons were constitutively immunoreactive for PJA1 (Fig. 6A–D). In SOD1-ALS spinal cord, however, cytoplasmic hyaline

inclusions in PJA1-immunoreactive anterior horn motor neurons were not immunostained for PJA1 (Fig. 6E). Similarly, brainstem-type and cortical Lewy bodies in PD cases were immunonegative for PJA1, while Marinesco bodies were lightly immunostained for PJA1 (Fig. 6F–H). Intranuclear polyglutamine inclusions in HD cases were not immunostained for PJA1 (Fig. 6I, J), whereas some of the intranuclear polyglutamine inclusions observed in MJD were immunostained for PJA1 (Fig. 6K, L). Double immunofluorescence staining of MJD neurons demonstrated some of the intranuclear polyglutamine inclusions were immunoreactive for PJA1 (Fig. 6M–O). Besides these pathological inclusions, immunostaining patterns for

(Figure legend continued from previous page.)

adenoviruses expressing DsRed- and FLAG-tagged genes of interest (GOI), i.e. human wild-type (WT) and P525L FUS (B), WT and G93A SOD1 (C), WT and A53T α -synuclein (D), ataxin-3 Q28 and Q84 (E), and huntingtin exon 1 Q23 and Q74 (F), and EGFP-tagged PJA1 or PJA1 Δ R, followed by incubation with 0.5 μ M MG-132. (B1–4) Suppression of FUS aggregate formation by PJA1. (B1) Western blot analysis of 1464R-derived neuronal cells infected with adenoviruses expressing DsRed- and FLAG-tagged human WT and P525L FUS (AxDsRhFUSWTF, AxDsRhFUSP525LFL) and EGFP-tagged PJA1 (AxpJA1EGFP) or PJA1 Δ R (AxpJA1 Δ REGFP) in the presence of MG-132. (B2) Densitometric analysis of FLAG Western blot data of RIPA-insoluble WT and P525L FUS versus PJA1 and PJA1 Δ R (PJA1D) (arrowheads in B1; $n = 3$) calibrated by GAPDH signals. Data are expressed as relative density compared with AxEGFP-treated control samples in the presence of MG132. Results are presented as mean \pm SD ($*P < 0.05$). (B3) The co-immunoprecipitation (Co-IP) assay showing that PJA1 and PJA1 Δ R bind to WT and P525L FUS that are ubiquitinated (arrowheads). (B4) Fluorescence microscopy of TuJ1-immunoreactive neurons infected with adenoviruses expressing DsRed-tagged human P525L FUS and EGFP-tagged human PJA1 in the presence of MG-132. The nucleus was counterstained with Hoechst 33342. (C1–4) Suppression of SOD1 aggregate formation by PJA1. (C1) Western blot analysis of 1464R-derived neuronal cells infected with adenoviruses expressing DsRed- and FLAG-tagged human WT and G93A SOD1 (AxDsRhSOD1WTF, AxDsRhSOD1G93AFL) and EGFP-tagged PJA1 (AxpJA1EGFP) or PJA1 Δ R (AxpJA1 Δ REGFP) in the presence of MG-132. (C2) Densitometric analysis of the FLAG Western blot data of RIPA-insoluble WT and G93A SOD1 versus PJA1 and PJA1 Δ R (PJA1D) (arrowheads in C1; $n = 3$) calibrated by GAPDH signals. Data are expressed as relative density compared with AxEGFP-treated control samples in the presence of MG132. Results are presented as mean \pm SD ($*P < 0.05$). (C3) The Co-IP assay showing that PJA1 and PJA1 Δ R bind to WT and G93A SOD1 that are ubiquitinated (arrowheads). (C4) Fluorescence microscopy of TuJ1-immunoreactive neurons infected with adenoviruses expressing DsRed-tagged human G93A SOD1 and EGFP-tagged human PJA1 in the presence of MG-132. The nucleus was counterstained with Hoechst 33342. (D1–4) Suppression of α -synuclein aggregate formation by PJA1. (D1) Western blot analysis of 1464R-derived neuronal cells infected with adenoviruses expressing DsRed- and FLAG-tagged human WT and A53T α -synuclein (AxDsRhSNCAWTF, AxDsRhSNCAA53TFL) and EGFP-tagged PJA1 (AxpJA1EGFP) or PJA1 Δ R (AxpJA1 Δ REGFP) in the presence of MG-132. (D2) Densitometric analysis of the FLAG and phosphorylated α -synuclein Western blot data of RIPA-insoluble WT and A53T α -synuclein versus PJA1 and PJA1 Δ R (PJA1D) (arrowheads in D1; $n = 3$) calibrated by GAPDH signals. Data are expressed as relative density compared with AxEGFP-treated control samples in the presence of MG132. Results are presented as mean \pm SD ($*P < 0.05$). (D3) The Co-IP assay showing that PJA1 and PJA1 Δ R bind to WT and A53T α -synuclein that are ubiquitinated (arrowheads). (D4) Fluorescence microscopy of TuJ1-immunoreactive neurons infected with adenoviruses expressing DsRed-tagged human A53T α -synuclein and EGFP-tagged human PJA1 in the presence of MG-132. The nucleus was counterstained with Hoechst 33342. (E1–4) Suppression of ataxin-3 aggregate formation by PJA1. (E1) Western blot analysis of 1464R-derived neuronal cells infected with adenoviruses expressing DsRed- and FLAG-tagged human ataxin-3 Q28 and Q84 (AxDsRhATXN3Q28FL, AxDsRhATXN3Q84FL) and EGFP-tagged PJA1 (AxpJA1EGFP) or PJA1 Δ R (AxpJA1 Δ REGFP) in the presence of MG-132. (E2) Densitometric analysis of the FLAG Western blot data of RIPA-insoluble ataxin-3 Q28 and Q84 versus PJA1 and PJA1 Δ R (PJA1D) (arrowheads in E1; $n = 3$) calibrated by GAPDH signals. Data are expressed as relative density compared with AxEGFP-treated control samples in the presence of MG132. Results are presented as mean \pm SD ($*P < 0.05$). (E3) The Co-IP assay showing that PJA1 and PJA1 Δ R bind to ataxin-3 Q28 and Q84 that are ubiquitinated (arrowheads). (E4) Fluorescence microscopy of 1464R-derived TuJ1-immunoreactive neurons infected with adenoviruses expressing DsRed-tagged human ataxin-3 Q84 and EGFP-tagged human PJA1 in the presence of MG-132. The nucleus was counterstained with Hoechst 33342. (F1–4) Suppression of ataxin-3 aggregate formation by PJA1. (F1) Western blot analysis of 1464R-derived neuronal cells infected with adenoviruses expressing DsRed- and FLAG-tagged huntingtin exon 1/Q23 and Q74 (AxDsRhHttEx1Q23FL, AxDsRhHttEx1Q74FL) and EGFP-tagged PJA1 (AxpJA1EGFP) or PJA1 Δ R (AxpJA1 Δ REGFP) in the absence or presence of MG-132. (F2) Densitometric analysis of the FLAG Western blot data of RIPA-insoluble huntingtin exon 1 Q23 and Q74 versus PJA1 and PJA1 Δ R (PJA1D) (arrowheads in F1; $n = 3$) calibrated by GAPDH signals. Data are expressed as relative density compared with AxEGFP-treated control samples in the presence of MG132. Results are presented as mean \pm SD ($*P < 0.05$). (E3) The Co-IP assay showing that PJA1 and PJA1 Δ R bind to huntingtin exon 1/Q23 and Q74 that are ubiquitinated (arrowheads). (E4) Fluorescence microscopy of 1464R-derived TuJ1-immunoreactive neurons infected with adenoviruses expressing DsRed-tagged human huntingtin exon 1 Q74 and EGFP-tagged human PJA1 in the presence of MG-132. The nucleus was counterstained with Hoechst 33342.

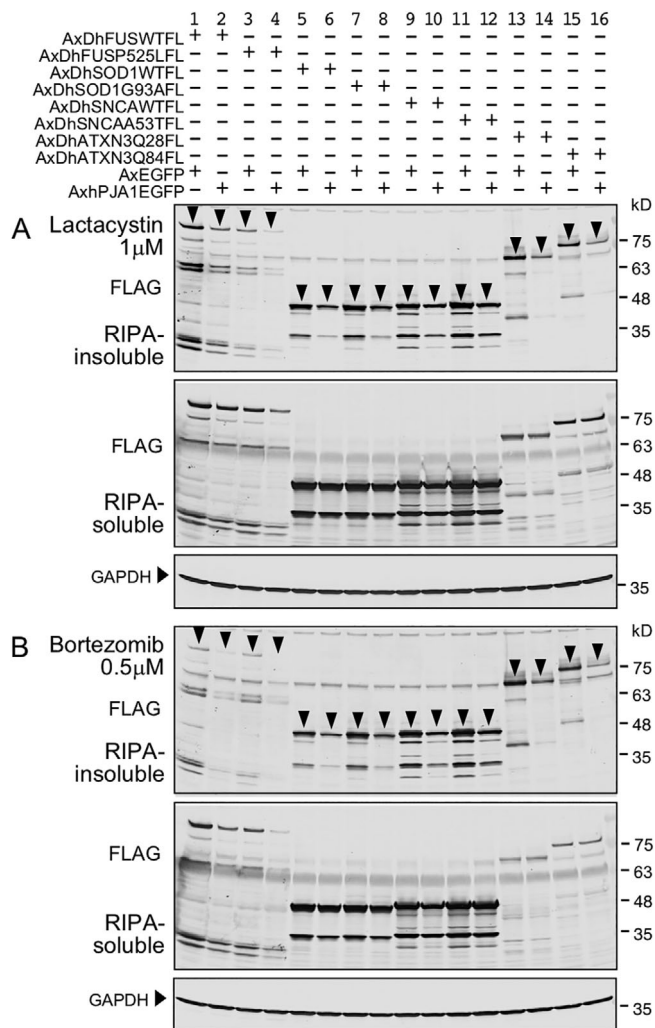


Fig. 4 Suppression of the aggregate formation of neurodegenerative disease-associated proteins by PJA1 in the presence of proteasome inhibitor lactacystin or bortezomib. FLAG Western blot analysis of 1464R-derived neurons infected with adenoviruses expressing DsRed- and FLAG-tagged human wild-type (WT) and P525L FUS, WT and G93A SOD1, WT and A53T α -synuclein, and ataxin-3 Q28 and G84 (arrowheads), and EGFP-tagged PJA1 in the presence of 1 μ M lactacystin (A) or 0.5 μ M bortezomib (B).

PJA1 in neurons did not differ between diseased and non-diseased control cases.

DISCUSSION

We have previously shown that adenovirally transduced cytoplasmic TDP-43 aggregate formation in 1464R-derived neuronal cells under proteasome inhibition was markedly suppressed by co-infection of adenoviruses expressing PJA1.¹⁶ PJA1, a RING-H2 finger E3 ubiquitin ligase abundantly expressed in the brain, ubiquitinates MAGED1/NRAGE/DIxin1 leading to its subsequent degradation by the proteasome,^{37–39} controls TGF- β /SMAD

signaling^{40–43} and promotes tumorigenesis of glioblastoma.^{44,45} The PJA1 gene is suggested to be one of the deficient genes responsible for neurodevelopmental disorders associated with craniofacial malformation and/or epilepsy.^{46,47} We have found that PJA1 binds to TDP-43 and suppresses the cytoplasmic TDP-43 aggregate formation, suggesting that PJA1 ubiquitinates and degrades TDP-43 through the ubiquitin-proteasome pathway.¹⁶ There have been several reports describing ubiquitinating enzymatic activities against TDP-43 that include Parkin,¹⁷ VHL/CUL2 E3 complex,¹⁸ RNF112/ZNF179¹⁹ and RNF220.²⁰ In these, Parkin ubiquitinates TDP-43 but promotes TDP-43 aggregate formation.¹⁷ VHL/CUL2 E3 complex ubiquitinates misfolded TDP-43 and promotes TDP-43 clearance.¹⁸ RNF112 E3 ubiquitinates TDP-43 and attenuates insoluble TDP-43 aggregates.¹⁹ More recently, RNF220 E3 ubiquitin ligase was reported to interact with TDP43 *in vitro* and *in vivo*, and promote its ubiquitination and proteasomal degradation.²⁰ In the present study, we examined Parkin/PARK2, RNF112/ZNF179 and RNF220, but failed to find their suppressive effects on adenoviral TDP-43 aggregate formation in our cultured neuronal cell models using 1464R cells, although, like PJA1, they all bind to ubiquitinated TDP-43 as verified by Co-IP. In our preliminary study, we did not observe the suppressive effects of RNF112 adenovirus on cytoplasmic TDP-43 aggregate formation in mouse facial motor neurons *in vivo* (Watabe *et al.*, unpublished data). Although detailed investigations are further required concerning differences in neural cell types and/or coupled E2 conjugating enzymes that may affect the specificity and efficiency of ubiquitination and proteasomal degradation, these results suggest that PJA1, but not Parkin, RNF112 or RNF220, is one of the major E3 ubiquitin ligases for TDP-43 to reduce its aggregation propensity in neuronal cells. In addition, PJA1, as well as HSF1, also suppressed the phosphorylation of RIPA-insoluble TDP-43 as demonstrated by Western blot. Pathomechanisms of TDP-43 phosphorylation are still unclear.⁴⁸ Although TDP-43 phosphorylation is consistently associated with its aggregation, a recent report described that TDP-43 phosphorylation may be a protective cellular response to counteract TDP-43 aggregation.⁴⁹

On the other hand, a recent report by Ghosh *et al.*²¹ revealed that PJA1 facilitates degradation of ataxin-3 and huntingtin polyglutamine proteins and suppresses polyglutamine-mediated toxicity, which suggests a possibility of common suppressive activity of PJA1 on the formation of protein aggregates in neurodegenerative diseases. Therefore, in the present study, we examined the suppressive effects of adenovirally transduced PJA1 on the adenovirus-induced aggregate formation of FUS, SOD1 and α -synuclein, as well as ataxin-3 and huntingtin

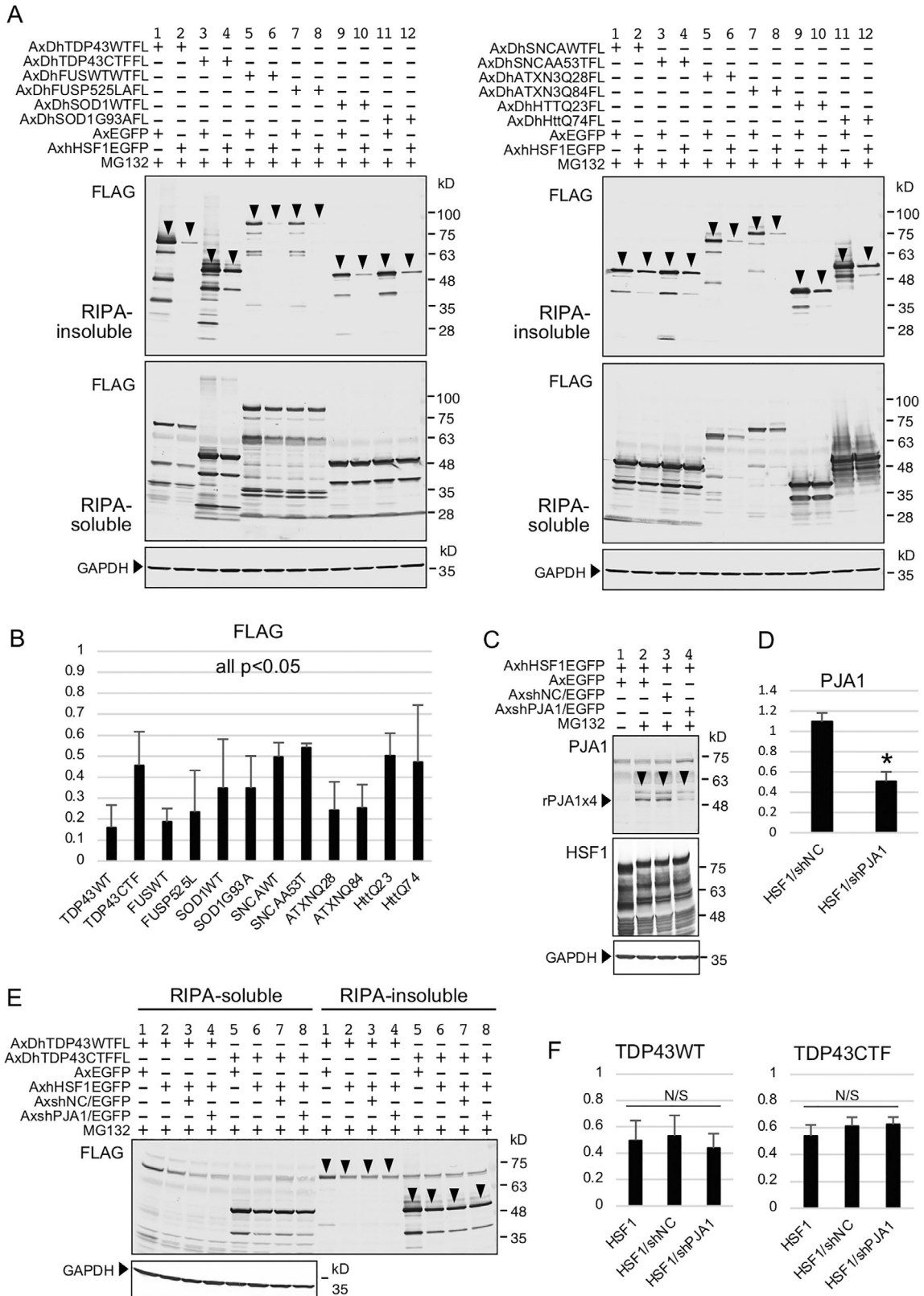


Fig. 5 Suppression of the aggregate formation of neurodegenerative disease-associated proteins by HSF1. (A) Western blot analysis of 1464R-derived neuronal cells infected with adenoviruses expressing DsRed- and FLAG-tagged human wild-type (WT) and C-terminal fragment (CTF) TDP-43, WT and P525L FUS, WT and G93A SOD1, WT and S53T α -synuclein, ataxin-3 Q28 and G84, and huntingtin (Figure legend continues on next page.)

polyglutamine proteins by Western blotting, and found that the RIPA-insoluble aggregate formation of all these neurodegeneration-associated proteins was consistently suppressed by PJA1 in our cultured neuronal cell models. Additionally, both WT PJA1 and PJA1 lacking RINF finger domain (PJA1 Δ R) suppressed phosphorylation of insoluble α -synuclein (Fig. 3D1,2), suggesting that PJA1 binding itself to α -synuclein partially interferes phosphorylation of α -synuclein, although the pathological significance of its phosphorylation remains unclear. Similarly, PJA1 Δ R adenovirus suppressed the aggregate formation of G93A SOD1 (Fig. 2C1,2), which may indicate that PJA1 binding itself also interferes with G93A SOD1 aggregation. Conversely, a previous report describing transcriptome analysis of G93A SOD1-expressing NSC34 motor neuron-like cells has shown elevated transcriptional expression of PJA1.⁵⁰

As for another ubiquitinating enzymatic activity that counteracts protein aggregation, it has been known that carboxy-terminus of Hsc70-interacting protein (CHIP), also called STUB1, has the dual function of co-chaperone and E3 ubiquitin ligase,⁵¹ and promotes degradation of multiple neurodegenerative disease-associated proteins that include α -synuclein,⁵² mutant (G93A) SOD1,⁵³ and expanded huntingtin and ataxin-3.^{54,55} Although E3 ubiquitin ligase for FUS has not been identified,⁵⁶ such functional redundancy of E3 ubiquitin ligases, i.e. PJA1 and CHIP, in this case, may facilitate efficient, continued and/or cell type-specific degradation of these substrates.⁵⁷ The functional difference between CHIP and PJA1 awaits further investigations.

It has been widely documented that HSF1 activity is impaired in the affected brain and spinal cords in patients with neurodegenerative diseases such as PD, ALS and HD, which leads to accumulation and aggregation of α -synuclein, TDP-43, SOD1 and polyglutamine proteins, respectively.²⁴ In the present study, we revealed that HSF1 suppresses the aggregate formation of TDP-43, FUS, SOD1, α -synuclein, ataxin-3 and huntingtin in our experimental protocols. However, we are unable to

demonstrate that the suppressive effects of HSF1 on the protein aggregate formation are solely due to endogenous PJA1 upregulation, because adenoviral transduction of shRNA for rat PJA1 knock-down did not inhibit the suppressive activity of HSF1 in the present study. Our previous study also showed that PJA1 Δ R did not act in a dominant-negative manner to inhibit WT PJA1 or HSF1 function.¹⁶ These results suggest that PJA1 is not solely responsible for suppressing the formation of disease-related protein aggregates as an effector molecule downstream of HSF1. Other downstream effector molecules such as a variety of heat shock proteins induced by HSF1 may cooperate to counteract the protein aggregate formation.²⁴ Conversely, co-aggregation of disease-linked proteins such as tau, α -synuclein, TDP-43 and huntingtin has been well recognized in diseased human brains, suggesting that common mechanisms of disease-associated protein aggregation may exist such as impairment of protein degradation machinery that includes ubiquitin-proteasome and autophagy systems.^{58–60}

The present immunohistochemical data showed that normal human brain and spinal cord neurons were immunoreactive for PJA1, whereas intracytoplasmic hyaline inclusions in SOD1-ALS motor neurons, brainstem-type and cortical Lewy bodies in PD neurons, and intranuclear inclusions in HD neurons were not immunostained for PJA1. Although some intranuclear inclusions in MJD were immunoreactive for PJA1, overall protein aggregates in diseased neurons were not immunostained for PJA1. These results suggest that PJA1 is constitutively expressed in the majority of neurons where pathological cytoplasmic or nuclear protein aggregates are formed, and the formation of mature inclusions is partially due to the consequence of the lack of protein degradation machinery that includes ubiquitin-proteasome pathway involving PJA1, although whether PJA1 prevents the development of protein oligomers or more mature cytoplasmic aggregates remains unknown. On the other hand, because all these disease-linked proteins are ubiquitously expressed in most somatic cells, PJA1 binding to these proteins may not be

(Figure legend continued from previous page.)

exon 1 Q23 and Q74 (arrowheads), and EGFP-tagged HSF1 in the presence of 0.5 μ M MG-132. (B) Densitometric analysis of FLAG Western blot data of RIPA-insoluble fractions versus PJA1 (arrowheads in A; $n = 3$) calibrated by GAPDH signals. Data are expressed as relative density compared with AxEGFP-treated control samples. Results are presented as mean \pm SD. All bars; $P < 0.05$. (C) Western blot analysis of 1464R-derived neuronal cells infected with adenoviruses expressing EGFP-tagged HSF1 and rat negative control (NC) or PJA1 shRNA/EGFP (AxshNC/EGFP, AxshPJA1/EGFP) in the presence of 0.5 μ M MG-132. (D) Densitometric analysis of PJA1 Western blot data (arrowheads in C; $n = 3$) calibrated by GAPDH signals. Data are expressed as relative density compared with AxEGFP-treated control samples in the presence of MG132. Results are presented as mean \pm SD ($*P < 0.05$). (E) Western blot analysis of 1464R-derived neuronal cells infected with adenoviruses expressing DsRed- and FLAG-tagged human WT and CTF TDP-43, EGFP-tagged HSF1 and rat NC or PJA1 shRNA/EGFP in the presence of 0.5 μ M MG-132. (F) Densitometric analysis of FLAG Western blot data of RIPA-insoluble WT and CTF TDP-43 (arrowheads in E; $n = 3$) calibrated by GAPDH signals. Data are expressed as relative density compared with AxEGFP-treated control samples in the presence of MG132. Results are presented as mean \pm SD (N/S; not significant).

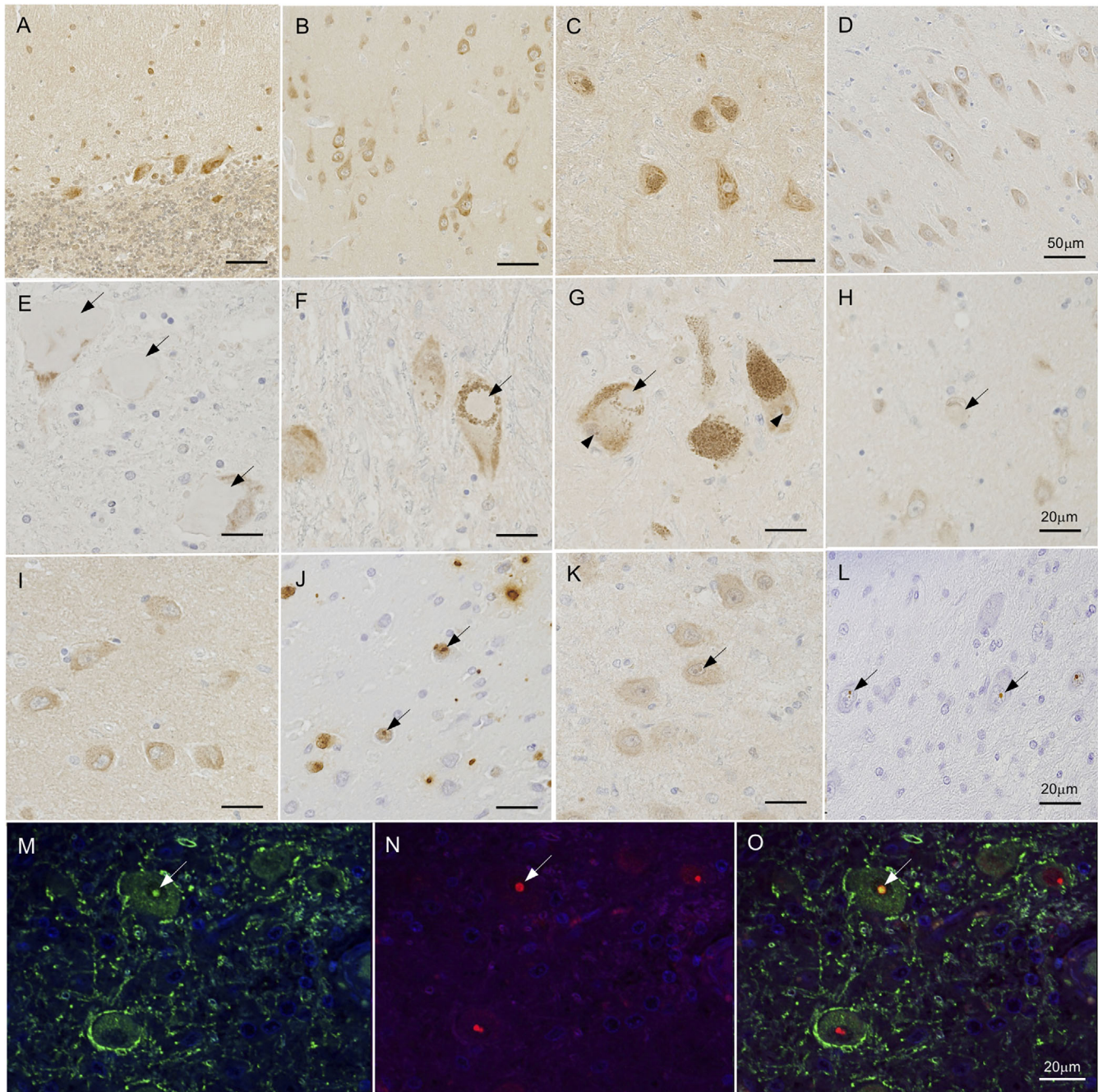


Fig. 6 Immunohistochemistry of PJA1 in human brains. (A–D) PJA1-immunoreactive cerebellar Purkinje cells (A), temporal cortical neurons (B), dopaminergic neurons in substantia nigra pars compacta (C), and hippocampal CA2 neurons (D) in a non-diseased 74-year-old male control case. (E) PJA1-immunoreactive anterior horn motor neurons containing PJA1-negative hyaline inclusions (arrows) in the cervical spinal cord in a SOD1-amyotrophic lateral sclerosis (ALS) case. (F, G) PJA1-immunoreactive, neuromelanin-bearing dopaminergic neurons containing PJA1-negative Lewy bodies (arrows) and PJA1-positive Marinesco bodies (arrowheads) in pars compacta of substantia nigra of a Parkinson's disease (PD) case. (H) A PJA1-immunoreactive neuron containing PJA1-negative cortical Lewy body in the amygdala of a PD case (arrow). (I, J) PJA1-immunoreactive neurons containing PJA1-negative (I), polyglutamine (1C2)-positive nuclear inclusions (J; arrows) in the amygdala of a Huntington's disease case. (K, L) A PJA1-immunoreactive pontine neuron containing PJA1- (K) and 1C2- (L) positive nuclear inclusions (arrows) in the pons of Machado–Joseph disease (MJD) case. (M–O) Double immunofluorescence of a pontine neuron containing PJA1- (M) and 1C2- (N) positive nuclear inclusions (arrows) in an MJD case. Scale bars: 50 μm (A–D); 20 μm (E–O).

specific to certain neuronal species characteristic of individual neurodegenerative diseases. It remains difficult to explain the cell type specificity responsible for the accumulation and aggregate formation of these disease-linked proteins.

There is growing acceptance of the view that the spreading of pathological protein aggregates composed of amyloid β , tau, α -synuclein, huntingtin and TDP-43 is the principal feature in the progression of AD, PD, HD, ALS and FTLN, respectively.^{1–7} The progression of symptoms in patients affected by these diseases deeply correlates with the spreading pathology of the representative protein aggregates in the brain and spinal cord. Therefore, suppressive effects of E3 ubiquitin ligases, such as PJA1, on protein aggregate formation may halt or slow disease progression, although *in vitro* adenoviral expression of PJA1 did not support cell survival after adenoviral TDP-43 expression and proteasome inhibition as shown in our previous study.¹⁶ Recently, strategies to target E3 ligases and discover activators of E3 ligases with ubiquitin variants have been reported and are expected to be used as therapeutic candidates for neurodegenerative diseases.^{61–63}

In summary, the present study demonstrated that PJA1 suppresses the aggregate formation of neurodegenerative disease-associated proteins that include TDP-43, FUS, SOD1, α -synuclein, ataxin-3 and huntingtin. These results suggest that PJA1 is a potential therapeutic target for neurodegenerative diseases that include ALS, FTLN, PD, MJD and HD.

ACKNOWLEDGMENTS

This work was supported by Grants-in-Aid for Scientific Research from the Ministry of Education, Culture, Sports, Science and Technology, Japan (JSPS KAKENHI) #18K06507 (to KW), and by the Collaborative Research Project (2020–2021) of Brain Research Institute, Niigata University.

DISCLOSURE

The authors declare no competing financial interests.

REFERENCES

- Prusiner SB. Biology and genetics of prions causing neurodegeneration. *Annu Rev Genet* 2013; **47**: 601–623.
- Brettschneider J, Del TK, Lee VM-Y, Trojanowski JQ. Spreading of pathology in neurodegenerative diseases: A focus on human studies. *Nat Rev Neurosci* 2015; **16**: 109–120.
- Lim J, Yue Z. Neuronal aggregates: Formation, clearance, and spreading. *Dev Cell* 2015; **32**: 491–501.
- Bourdenx M, Koulakiotis NS, Sanoudou D, Bezard E, Dehay B, Tsarbopoulos A. Protein aggregation and neurodegeneration in prototypical neurodegenerative diseases: Examples of amyloidopathies, tauopathies and synucleinopathies. *Prog Neurobiol* 2017; **155**: 171–193.
- Davis AA, CEG L, Holtzman DM. Intercellular spread of protein aggregates in neurodegenerative disease. *Annu Rev Cell Dev Biol* 2018; **34**: 545–568.
- Jucker M, Walker LC. Propagation and spread of pathogenic protein assemblies in neurodegenerative diseases. *Nat Neurosci* 2018; **21**: 1341–1349.
- Peng C, Trojanowski JQ, Lee VM. Protein transmission in neurodegenerative disease. *Nat Rev Neurol* 2020; **16**: 199–212.
- Blokhuis AM, Groen EJ, Koppers M, van den Berg LH, Pasterkamp RJ. Protein aggregation in amyotrophic lateral sclerosis. *Acta Neuropathol* 2013; **125**: 777–794.
- Berning BA, Walker AK. The pathobiology of TDP-43 C-terminal fragments in ALS and FTLN. *Front Neurosci* 2019; **13**: 335.
- Hergesheimer RC, Chami AA, Assis DRD, Vourc P, Andres CR, Corcia P. The debated toxic role of aggregated TDP-43 in amyotrophic lateral sclerosis: A resolution in sight? *Brain* 2019; **142**: 1176–1194.
- Prasad A, Bharathi V, Sivalingam V, Girdhar A, Patel BK. Molecular mechanisms of TDP-43 misfolding and pathology in amyotrophic lateral sclerosis. *Front Mol Neurosci* 2019; **12**: 25.
- Portz B, Lee BL, Shorter J. FUS and TDP-43 phases in health and disease. *Trends Biochem Sci* 2021; **46**: 550–563.
- Keating SS, San Gil R, Swanson MEV, Scotter EL, Walker AK. TDP-43 pathology: From noxious assembly to therapeutic removal. *Prog Neurobiol* 2022; **211**: 102229. <https://doi.org/10.1016/j.pneurobio.2022.102229>
- Watabe K, Akiyama K, Kawakami E *et al.* Adenoviral expression of TDP-43 and FUS genes and shRNAs for protein degradation pathways in rodent motoneurons *in vitro* and *in vivo*. *Neuropathology* 2014; **34**: 83–98.
- Ishii T, Kawakami E, Endo K, Misawa H, Watabe K. Formation and spreading of TDP-43 aggregates in cultured neuronal and glial cells demonstrated by time-lapse imaging. *PLoS One* 2017; **12**: e0179375.
- Watabe K, Kato Y, Sakuma M *et al.* Praja1 RING-finger E3 ubiquitin ligase suppresses neuronal cytoplasmic TDP-43 aggregate formation. *Neuropathology* 2020; **40**: 570–586.
- Hebron ML, Lonskaya I, Sharpe K *et al.* Parkin ubiquitinates tar-DNA binding protein-43 (TDP-43) and promotes its cytosolic accumulation via interaction with histone deacetylase 6 (HDAC6). *J Biol Chem* 2013; **288**: 4103–4115.

18. Uchida T, Tamaki Y, Ayaki T *et al.* CUL2-mediated clearance of misfolded TDP-43 is paradoxically affected by VHL in oligodendrocytes in ALS. *Sci Rep* 2016; **6**: 19118.
19. Lee YC, Huang WC, Lin JH *et al.* Znf179 E3 ligase-mediated TDP-43 polyubiquitination is involved in TDP-43-ubiquitinated inclusions (UBI) (+)-related neurodegenerative pathology. *J Biomed Sci* 2018; **25**: 76.
20. Ma P, Li Y, Wang H, Mao B. Haploinsufficiency of the TDP43 ubiquitin E3 ligase RNF220 leads to ALS-like motor neuron defects in the mouse. *J Mol Cell Biol* 2021; **13**: 374–382.
21. Ghosh B, Karmakar S, Prasad M, Mandal AK. Prajal ubiquitin ligase facilitates degradation of polyglutamine proteins and suppresses polyglutamine-mediated toxicity. *Mol Biol Cell* 2021; **32**: 1579–1593.
22. Ishii T, Kawakami E, Endo K, Misawa H, Watabe K. Myelinating cocultures of rodent stem cell line-derived neurons and immortalized Schwann cells. *Neuropathology* 2017; **37**: 475–481.
23. Hooper PL, Durham HD, Török Z, Hooper PL, Crul T, Vigh L. The central role of heat shock factor 1 in synaptic fidelity and memory consolidation. *Cell Stress Chaperones* 2016; **21**: 745–753.
24. Gomez-Pastor R, Burchfiel ET, Thiele DJ. Regulation of heat shock transcription factors and their roles in physiology and disease. *Nat Rev Mol Cell Biol* 2018; **19**: 4–19.
25. Huang C, Wu J, Xu L, Wang J, Chen Z, Yang R. Regulation of HSF1 protein stabilization: An updated review. *Eur J Pharmacol* 2018; **822**: 69–77.
26. Chen HJ, Mitchell JC, Novoselov S *et al.* The heat shock response plays an important role in TDP-43 clearance: Evidence for dysfunction in amyotrophic lateral sclerosis. *Brain* 2016; **139**: 1417–1432.
27. Lin PY, Folorunso O, Tagliatalata G, Pierce A. Overexpression of heat shock factor 1 maintains TAR DNA binding protein 43 solubility via induction of inducible heat shock protein 70 in cultured cells. *J Neurosci Res* 2016; **682**: 671–682.
28. Lin PY, Simon SM, Koh WK, Folorunso O, Umbaugh CS, Pierce A. Heat shock factor 1 overexpression protects against exposure of hydrophobic residues on mutant SOD1 and early mortality in a mouse model of amyotrophic lateral sclerosis. *Mol Neurodegener* 2013; **8**: 43.
29. Watanabe S, Ageta-Ishihara N, Nagatsu S *et al.* SIRT1 overexpression ameliorates a mouse model of SOD1-linked amyotrophic lateral sclerosis via HSF1/HSP70i chaperone system. *Mol Brain* 2014; **7**: 62.
30. Wright GSA. Molecular and pharmacological chaperones for SOD1. *Biochem Soc Trans* 2020; **48**: 1795–1806.
31. Liangliang X, Yonghui H, Shunmei E, Shoufang G, Wei Z, Jiangying Z. Dominant-positive HSF1 decreases alpha-synuclein level and alpha-synuclein-induced toxicity. *Mol Biol Rep* 2010; **37**: 1875–1881.
32. Kilpatrick K, Novoa JA, Hancock T *et al.* Chemical induction of Hsp70 reduces α -synuclein aggregation in neuroglioma cells. *ACS Chem Biol* 2013; **8**: 1460–1468.
33. Kim E, Wang B, Sastry N *et al.* NEDD4-mediated HSF1 degradation underlies α -synucleinopathy. *Hum Mol Genet* 2016; **25**: 211–222.
34. Teixeira-Castro A, Ailion M, Jalles A *et al.* Neuron-specific proteotoxicity of mutant ataxin-3 in *C. elegans*: Rescue by the DAF-16 and HSF-1 pathways. *Hum Mol Genet* 2011; **20**: 2996–3009.
35. McLoughlin HS, Moore LR, Paulson HL. Pathogenesis of SCA3 and implications for other polyglutamine diseases. *Neurobiol Dis* 2020; **134**: 104635.
36. Gomez-Pastor R, Burchfiel ET, Neef DW *et al.* Abnormal degradation of the neuronal stress-protective transcription factor HSF1 in Huntington's disease. *Nat Commun* 2017; **8**: 14405.
37. Mishra L, Tully RE, Monga SP *et al.* Prajal, a novel gene encoding a RING-H2 motif in mouse development. *Oncogene* 1997; **15**: 2361–2368.
38. Sasaki A, Masuda Y, Iwai K, Ikeda K, Watanabe K. A RING finger protein Prajal regulates Dlx5-dependent transcription through its ubiquitin ligase activity for the dlx/Msx-interacting MAGE/Necdin family protein, Dlxin-1. *J Biol Chem* 2002; **277**: 22541–22546.
39. Zoabi M, Sadeh R, Bie PD, Ciechanover A. PRAJA1 is a ubiquitin ligase for the polycomb repressive complex 2 proteins. *Biochem Biophys Res Commun* 2011; **408**: 393–398.
40. Mishra L, Katuri V, Evans S. The role of PRAJA and ELF in TGF-beta signaling and gastric cancer. *Cancer Biol Ther* 2005; **4**: 694–699.
41. Saha T, Vardhini D, Tang Y *et al.* RING finger-dependent ubiquitination by PRAJA is dependent on TGF- β and potentially defines the functional status of the tumor suppressor ELF. *Oncogene* 2006; **25**: 693–705.
42. Chen J, Mitra A, Li S *et al.* Targeting the E3 ubiquitin ligase PJA1 enhances tumor-suppressing TGF β signaling. *Cancer Res* 2020; **80**: 1819–1832.
43. Ohshiro K, Chen J, Srivastav J, Mishra L, Mishra B. Alterations in TGF- β signaling leads to high HMG A2 levels potentially through modulation of PJA1/SMAD3 in HCC cells. *Genes Cancer* 2020; **11**: 43–52.
44. Shin J, Mishra V, Glasgow E *et al.* PRAJA is overexpressed in glioblastoma and contributes to neural precursor development. *Genes Cancer* 2017; **8**: 640–649.
45. Bunda S, Heir P, Metcalf J *et al.* CIC protein instability contributes to tumorigenesis in glioblastoma. *Nat Commun* 2019; **10**: 661.

46. Wieland I, Weidner C, Ciccone R *et al.* Contiguous gene deletions involving EFNB1, OPHN1, PJA1 and EDA in patients with craniofrontonasal syndrome. *Clin Genet* 2007; **72**: 506–516.
47. Suzuki T, Suzuki T, Raveau M *et al.* A recurrent PJA1 variant in trigonocephaly and neurodevelopmental disorders. *Ann Clin Transl Neurol* 2020; **7**: 1117–1131.
48. Eck RJ, Kraemer BC, Liachko NF. Regulation of TDP-43 phosphorylation in aging and disease. *GeroScience* 2021; **43**: 1605–1614.
49. Gruijs da Silva LA, Simonetti F, Hutten S *et al.* Disease-linked TDP-43 hyperphosphorylation suppresses TDP-43 condensation and aggregation. *EMBO J* 2022; **41**: e108443. <https://doi.org/10.15252/embj.2021108443>
50. Kirby J, Halligan E, Baptista MJ *et al.* Mutant SOD1 alters the motor neuronal transcriptome: Implications for familial ALS. *Brain* 2005; **128**: 1686–1706.
51. Zhang S, Hu ZW, Mao CY, Shi CH, Xu YM. CHIP as a therapeutic target for neurological diseases. *Cell Death Dis* 2020; **11**: 727.
52. Shin Y, Klucken J, Patterson C, Hyman BT, McLean PJ. The co-chaperone carboxyl terminus of Hsp70-interacting protein (CHIP) mediates α -synuclein degradation decisions between proteasomal and lysosomal pathways. *J Biol Chem* 2005; **280**: 23727–23734.
53. Urushitani M, Kurisu J, Tateno M *et al.* CHIP promotes proteasomal degradation of familial ALS-linked mutant SOD1 by ubiquitinating Hsp/Hsc70. *J Neurochem* 2004; **90**: 231–244.
54. Jana NR, Dikshit P, Goswami A *et al.* Co-chaperone CHIP associates with expanded polyglutamine protein and promotes their degradation by proteasomes. *J Biol Chem* 2005; **280**: 11635–11640.
55. Miller VM, Nelson RF, Gouvion CM *et al.* CHIP suppresses polyglutamine aggregation and toxicity in vitro and in vivo. *J Neurosci* 2005; **25**: 9152–9161.
56. Farina S, Esposito F, Battistoni M, Biamonti G, Francia S. Post-translational modifications modulate proteinopathies of TDP-43, FUS and hnRNP-A/B in amyotrophic lateral sclerosis. *Front Mol Biosci* 2021; **8**: 693325.
57. Rubenstein EM, Hochstrasser M. Redundancy and variation in the ubiquitin-mediated proteolytic targeting of a transcription factor. *Cell Cycle* 2010; **9**: 4282–4285.
58. Nonaka T, Masuda-Suzukake M, Hasegawa M. Molecular mechanisms of the co-deposition of multiple pathological proteins in neurodegenerative diseases. *Neuropathology* 2018; **38**: 64–71.
59. Coudert L, Nonaka T, Bernard E, Hasegawa M, Schaeffer L, Leblanc P. Phosphorylated and aggregated TDP-43 with seeding properties are induced upon mutant huntingtin (mHtt) polyglutamine expression in human cellular models. *Cell Mol Life Sci* 2019; **76**: 2615–2632.
60. Dewan R, Chia R, Ding J *et al.* Pathogenic huntingtin repeat expansions in patients with frontotemporal dementia and amyotrophic lateral sclerosis. *Neuron* 2021; **109**: 448–460.
61. Huang X, Dixit VM. Drugging the undruggables: Exploring the ubiquitin system for drug development. *Cell Res* 2016; **26**: 484–498.
62. Gabrielsen M, Buetow L, Nakasone MA *et al.* A general strategy for discovery of inhibitors and activators of RING and U-box E3 ligases with ubiquitin variants. *Mol Cell* 2017; **68**: 456–470.
63. Schmidt MF, Gan ZY, Komander D, Dewson G. Ubiquitin signalling in neurodegeneration: Mechanisms and therapeutic opportunities. *Cell Death Differ* 2021; **28**: 570–590.